to be studied, BACE and γ-secretase inhibitors are useful to reduce intracellular Aβ_{42} as well as extracellular Aβ, and may be important therapeutic tools for FAD with *PS1* gene mutations.

ACKNOWLEDGMENTS

REFERENCES

[1] Walsh DM, Klyubin I, Fadeeva JV, Rowen MJ, Selkoe DJ (2002) Amyloid-β oligomers: their production, toxicity and therapeutic inhibition. *Biochem Soc Trans* 30, 552-557.

[2] Gandy S (2005) The role of cerebral amyloid β accumulation in common forms of Alzheimer disease. *J Clin Invest* 115, 1121-1129.

[3] D'Andrea MR, Nagele RG, Wang HY, Peterson PA, Lee DH (2001) Evidence that neurons accumulating amyloid can undergo lysis to form amyloid plaques in Alzheimer's disease. *Histopathology* 38, 120-134.

[4] Gouras GK, Tsai J, Naslund J, Vincent B, Edgar M, Checler F, Greenfield JP, Haroutunian V, Buxbaum JD, Xu H, Greengard P, Relkin NR (2000) Intraneuronal Aβ42 accumulation in human brain. *Am J Pathol* 156, 15-20.

[5] Gyure KA, Durham R, Stewart WF, Smialek JE, Troncoso JC (2001) Intraneuronal Aβ-amyloid precedes development of amyloid plaques in Down syndrome. *Arch Pathol Lab Med* 125, 489-492.

[6] Mori C, Spooner ET, Wisniewski E, Wisniewski TM, Yamaguchi H, Saido TC, Tolan DR, Selkoe DJ, Lemere CA (2002) Intraneuronal Aβ42 accumulation in Down syndrome brain. *Amyloid* 9, 88-102.

[7] Chui DH, Tanahashi H, Ozawa K, Ikeda S, Checler F, Ueda O, Suzuki H, Araki W, Inoue H, Shirotani K, Takahashi K, Gallyas F, Tabira T (1999) Transgenic mice with Alzheimer presenilin 1 mutations show accelerated neurodegeneration without amyloid plaque formation. *Nat Med* 5, 560-564.

[8] Wirths O, Multhaup G, Czech C, Blanchard V, Moussaoui S, Tremp G, Pradier L, Beyreuther K, Bayer T (2001) Intraneuronal Aβ accumulation precedes plaque formation in β-amyloid precursor protein and presenilin-1 double-transgenic mice. *Neurosci Lett* 306, 116-120.

[9] Oddo S, Caccamo A, Shepherd JD, Murphy MP, Golde TE, Kayed R, Metherate R, Mattson MP, Akbari Y, LaFerla FM (2003) Triple-transgenic model of Alzheimer's disease with plaques and tangles: intracellular Aβ and synaptic dysfunction. *Neuron* 39, 409-421.

[10] Oakley H, Cole SL, Logan S, Maus E, Shao P, Craft J, Guillozet-Bongaarts A, Ohno M, Disterhoft J, Van Eldik L, Berry R, Vassar R (2006) Intraneuronal β-amyloid aggregates, neurodegeneration, and neuron loss in transgenic mice with five familial Alzheimer's disease mutations: potential factors in amyloid plaque formation. *J Neurosci* 26, 10129-10140.

[11] Ohyagi Y, Yamada T, Nishioka K, Clarke NJ, Tomlinson AJ, Naylor S, Nakabeppu Y, Kira J, Younkin SG (2000) Selective increase in cellular Aβ42 is related to apoptosis but not necrosis. *Neuroreport* 11, 167-171.

[12] Chui DH, Dobo E, Makifuchi T, Akiyama H, Kawakatsu S, Petit A, Checler F, Araki W, Takahashi K, Tabira T (2001) Apoptotic neurons in Alzheimer's disease frequently show intracellular Aβ42 labeling. *J Alzheimers Dis* 3, 231-239.

[13] Kienlen-Campard P, Miolet S, Tasiaux B, Octave J-N (2002) Intracellular amyloid-β 1-42, but not extracellular soluble amyloid-β peptides, induces neuronal apoptosis. *J Biol Chem* 277, 15666-15670.

[14] Kienlen-Campard P, Octave J-N (2002) Correlation between β-amyloid peptide production and human APP-induced neuronal death. *Peptides* 23, 1199-1204.

[15] Zhang Y, McLaughlin R, Goodyer C, LeBlanc A (2002) Selective cytotoxicity of intracellular amyloid β peptide 1-42 through p53 and Bax in cultured primary human neurons. *J Cell Biol* 156, 519-529.

[16] Rocchi A, Pellegrini S, Siciliano G, Murri L (2003) Causative and susceptibility genes for Alzheimer's disease: a review. *Brain Res Bull* 61, 1-24.

[17] Selkoe DJ (2001) Alzheimer's disease: genes, proteins, and therapy. *Physiol Rev* 81, 741-766.

[18] Katayama T, Imaizumi K, Manabe T, Hitomi J, Kudo T, Tohyama M (2004) Induction of neuronal death by ER stress in Alzheimer's disease. *J Chem Neuroanat* 28, 67-78.

[19] McCarthy JV (2005) Involvement of presenilins in cell-survival signalling pathways. *Biochem Soc Trans* 33, 568-572.

[20] Thinakaran G, Sisodia SS (2006) Presenilins and Alzheimer disease: the calcium conspiracy. *Nat Neurosci* 9, 1354-1355.

[21] Lakshmana MK, Araki W, Tabira T (2005) Amyloid β peptide binds a novel death-inducing protein, AB-DIP. *FASEB J* 19, 1362-1364.

[22] Ohyagi Y, Asahara H, Chui DH, Tsuruta Y, Sakae N, Miyoshi K, Yamada T, Kikuchi H, Taniwaki T, Murai H, Ikezoe K, Furuya H, Kawarabayashi T, Shoji M, Checler F, Iwaki T, Makifuchi T, Takeda K, Kira J, Tabira T (2005) Intracellular Aβ42 activates p53 promoter: a pathway to neurodegeneration in Alzheimer's disease. *FASEB J* 19, 255-257.

[23] Ohyagi Y, Tabira T (2006) Intracellular amyloid β-protein and its associated molecules in the pathogenesis of Alzheimer's disease. *Mini Rev Med Chem* 6, 1075-1080.

[24] Alves da Costa C, Sunyach C, Pardossi-Piquard R, Sevalle J, Vincent B, Boyer N, Kawarai T, Girardot N, St George-Hyslop P, Checler F (2006) Presenilin-dependent γ-secretase-mediated control of p53-associated cell death in Alzheimer's disease. *J Neurosci* 26, 6377-6385.

[25] Haupt S, Berger M, Goldberg Z, Haupt Y (2003) Apoptosis - the p53 network. *J Cell Sci* 116, 4077-4085.

[26] Romer L, Klein C, Dehner A, Kessler H, Buchner J (2006) p53–a natural cancer killer: Structural insights and therapeutic concepts. *Angew Chem Int Ed Engl* 45, 6440-6460.

[27] Vogelstein B, Lane D, Levine AJ (2000) Surfing the p53 network. *Nature* 408, 307-310.

[28] Miyoshi K, Ohyagi Y, Sakae N, Motomura K, Ma L, Taniwaki T, Furuya H, Tabira T, Kira J (2009) Enhancement of activation of caspases by presenilin 1 gene mutations and its inhibition by secretase inhibitors. *J Alzheimers Dis* 16, 551-564.

[29] Shirotani K, Takahashi K, Tabira T (1999) Effects of presenilin N-terminal fragments on production of amyloid β peptide and accumulation of endogenous presenilins. *Neurosci Lett* 262, 37-40.

[30] Hamano T, Muto T, Tabira T, Araki W, Kuriyama M, Mihara T, Yano S, Yamamoto H (2005) Abnormal intracellular trafficking of high affinity nerve growth factor receptor, Trk, in stable transfectants expressing presenilin 1 protein. *Mol Brain Res* **137**, 70-76.

[31] Takeda K, Araki W, Tabira T (2004) Enhanced generation of intracellular Aβ42 amyloid peptide by mutation of presenilins PS1 and PS2. *Eur J Neurosci* **19**, 258-264.

[32] Capell A, Meyn L, Fluhrer R, Teplow DB, Walter J, Haass C (2002) Apical sorting of β-secretase limits amyloid β-peptide production. *J Biol Chem* **277**, 5637-5643.

[33] Shearman MS, Beher D, Clarke EE, Lewis HD, Harrison T, Hunt P, Nadin A, Smith AL, Stevenson G, Castro JL (2000) L-685458, an aspartyl protease transition state mimic, is a potent inhibitor of amyloid β-protein precursor γ-secretase activity. *Biochemistry* **39**, 8698-8704.

[34] Wiltfang J, Esselmann H, Cupers P, Neumann M, Kretzschmar H, Beyermann M, Schleuder D, Jahn H, Rüther E, Kornhuber J, Annaert W, De Strooper B, Saftig P (2001) Elevation of β-amyloid peptide 2-42 in sporadic and familial Alzheimer's disease and its generation in PS1 knockout cells. *J Biol Chem* **276**, 42645-42657.

[35] Almeida CG, Takahashi RH, Gouras GK (2006) β-amyloid accumulation impairs multivesicular body sorting by inhibiting the ubiquitin-proteasome system. *J Neurosci* **26**, 4277-4288.

[36] Koo EH, Kopan R (2004) Potential role of presenilin-regulated signaling pathways in sporadic neurodegeneration. *Nat Med* **10 Suppl**, S26-S33.

[37] Nguyen HN, Lee MS, Hwang DY, Kim YK, Yoon DY, Lee JW, Yun YP, Lee MK, Oh KW, Hong JT (2007) Mutant presenilin 2 increased oxidative stress and p53 expression in neuronal cells. *Biochem Biophys Res Commun* **357**, 174-180.

[38] LaFerla FM, Green KN, Oddo S (2007) Intracellular amyloid-β in Alzheimer's disease. *Nature Rev* **8**, 499-509.

[39] Tashiro J, Kikuchi S, Shinpo K, Kishimoto R, Tsuji S, Sasaki H (2007) Role of p53 in neurotoxicity induced by the endoplasmic reticulum stress agent tunicamycin in organotypic slice cultures of rat spinal cord. *J Neurosci Res* **85**, 395-401.

[40] Zhu X, Raina AK, Perry G, Smith MA (2004) Alzheimer's disease: the two-hit hypothesis. *Lancet Neurol* **3**, 219-226.

[41] Cicconi S, Gentile A, Ciotti MT, Parasassi T, Serafino A, Calissano P (2007) Apoptotic death induces Aβ production and fibril formation to a much larger extent than necrotic-like death in CGNs. *J Alzheimers Dis* **12**, 211-220.

[42] Billings LM, Oddo S, Green KN, McGaugh JL, LaFerla FM (2005) Intraneuronal Aβ causes the onset of early Alzheimer's disease-related cognitive deficits in transgenic mice. *Neuron* **45**, 675-688.

[43] Hol EM, Van Leeuwen FW, Fischer DF (2005) The proteasome in Alzheimer's disease and Parkinson's disease: lessons from ubiquitin B+1. *Trends Mol Med* **11**, 488-495.

[44] Van Leeuwen FW, De Kleijn DP, Van den Hurk HH, Neubauer A, Sonnemans MA, Sluijs JA, Köycü S, Ramdjielal RD, Salehi A, Martens GJ, Grosveld FG, Peter J, Burbach H, Hol EM (1998) Frameshift mutants of β amyloid precursor protein and ubiquitin-B in Alzheimer's and Down patients. *Science* **279**, 242-247.

[45] Van Leeuwen FW, Van Tijn P, Sonnemans MA, Hobo B, Mann DM, Van Broeckhoven C, Kumar-Singh S, Cras P, Leuba G, Savioz A, Maat-Schieman ML, Yamaguchi H, Kros JM, Kamphorst W, Hol EM, De Vos RA, Fischer DF (2006) Frameshift proteins in autosomal dominant forms of Alzheimer disease and other tauopathies. *Neurology* **66 (2 Suppl 1)**, S86-S92.

ORIGINAL PAPER

Amyloid-β accumulation caused by chloroquine injections precedes ER stress and autophagosome formation in rat skeletal muscle

Koji Ikezoe · Hirokazu Furuya · Hajime Arahata ·
Masahiro Nakagawa · Takahisa Tateishi ·
Naoki Fujii · Jun-ichi Kira

Abstract Chloroquine, an anti-malaria drug, is known to cause myopathy with rimmed vacuole formation. Although it disrupts the lysosomal degradation of proteins, the precise mechanism underlying muscle fiber degeneration has remained unclear. We investigated the temporal profiles of muscle fiber degeneration in chloroquine-treated rats, paying special attention to endoplasmic reticulum (ER) stress and autophagy. Male Wistar rats were intraperitoneally injected with chloroquine diphosphate at a dosage of 50 mg/kg body weight every day. We examined the localization and levels of proteins related to ER stress and autophagy in soleus muscle by means of immunohistochemistry and Western blotting at 3, 5, and 7 weeks after the beginning of the treatment. At 3 weeks, the levels of LC3-II and amyloid-β (Aβ) were increased. At 5 weeks, an unfolded protein response took place. At 7 weeks, rimmed vacuole formation became obvious. Interestingly, SERCA2, a Ca2+ -pump ATPase located in the endoplasmic/sarcoplasmic reticulum membrane was up-regulated at 5 weeks after treatment, but declined to the control level by 7 weeks. Taken together, these findings suggest that Aβ accumulation (at 3 weeks) caused by the disruption of lysosomal enzymes precedes an unfolded protein response (at 5 weeks). Next, activation of autophagy occurs (at 7 weeks), probably using sarcoplasmic reticulum membrane, the amount of which was increased. Chloroquine-treated rats could be useful for investigating the pathogenesis of diseases related to Aβ accumulation.

Introduction

It is well known that myopathies with rimmed vacuoles, such as inclusion body myositis (IBM), share several pathological characteristics with the Alzheimer's disease (AD) brain, namely accumulation of amyloid-β (Aβ) and phosphorylated tau [2, 3]. Although the pathogenesis of AD is complicated, the accumulation of Aβ is thought to be a primary cause leading to the neuronal degeneration in AD (amyloid cascade hypothesis) [14]. Similarly, intrasarcoplasmic accumulation of Aβ seems to evoke muscle fiber degeneration with vacuolar formation [39]. Indeed, experimental excessive production of Aβ precursor protein (APP) [1] or Aβ [12, 19] causes muscle fiber degeneration with rimmed vacuoles.

The precise mechanisms underlying the neuronal and muscle fiber degeneration caused by Aβ are not understood. However, it has been reported that accumulation of insoluble Aβ leads to the formation of unfolded or misfolded proteins [33] and disturbs intracellular Ca2+ homeostasis [9]. Disturbed intracellular Ca2+ homeostasis disrupts ER functions, resulting in further accumulation of unfolded or misfolded proteins in the endoplasmic reticulum (ER) lumen, a process known as ER stress [18, 26]. Under ER stress, the unfolded protein response (UPR) [29, 43] and ER-associated

K. Ikezoe (✉) · H. Arahata · T. Tateishi · J. Kira
Department of Neurology, Neurological Institute,
Graduate School of Medical Sciences, Kyushu University,
3-1-1 Maidashi, Higashi-ku, Fukuoka 812-8582, Japan
e-mail: kikezoe@neuro.med.kyushu-u.ac.jp

K. Ikezoe · H. Furuya · H. Arahata · N. Fujii
Department of Neurology, National Omuta Hospital,
Omuta, Fukuoka, Japan

M. Nakagawa
Department of Plastic Surgery, Shizuoka Cancer Center,
Nagaizumi, Shizuoka, Japan

Springer

degradation (ERAD) [27] are evoked. If cells cannot resolve ER stress using UPR and ERAD, they undergo apoptotic cell death via caspase-12 activation [31]. Indeed, ER stress is evoked in muscles with Aβ accumulation owing to IBM [41].

Yu et al. [44] reported that autophagy is activated in the AD brain. In the muscle fibers of patients with myopathies with rimmed vacuoles, increased autophagy is also observed [37]. Autophagy, especially macroautophagy, is a process of bulk degradation of cytoplasmic components by engulfing whole portions of cytoplasm together with various organelles [35]. During this process, cytoplasmic constituents are sequestered into double-membraned vesicles named autophagosomes. These autophagosomes then fuse with lysosomes, resulting in the formation of single-membraned autolysosomes or autophagolysosomes, within the lumens of which the contents are degraded by lysosomal enzymes [22]. In mammalian cells, the microtubule-associated protein light chain 3 (LC3) is essential for the formation of the autophagosome membrane (isolation membrane). The cytosolic form of LC3 (LC3-I) is converted to an autophagosome membrane-associated form, LC3-II, in an early step in the autophagy process [28].

Together, the activations of ER stress and autophagy seem to be evoked to deal with Aβ accumulation in skeletal muscle cells showing rimmed vacuole formation. It has been reported that several myopathies with [3] or without [16, 30] rimmed vacuoles are related to ER stress. However, the relationship between autophagy and the ER stress in myopathies with rimmed vacuoles remains to be examined.

Chloroquine, an anti-malaria drug, raises the pH in lysosomal lumens, and causes the disruption of lysosomal function [36]. It is well known that long-term administration of chloroquine causes myopathy with rimmed vacuole formation [24]. In this study, we examined the temporal profiles of ER stress and autophagy during muscle fiber degeneration in chloroquine-treated rats to assess the relationship between these processes.

Materials and methods

Chloroquine-treated rats

We prepared chloroquine-treated rats as follows: male Wistar rats (2 weeks old) were injected intraperitoneally with chloroquine diphosphate at a dosage of 50 mg/kg body weight every day. They were killed 3 ($n = 3$), 5 ($n = 3$), and 7 ($n = 3$) weeks after the beginning of the treatment. Untreated 5-week-old male Wistar rats were also employed in this study as normal controls. All animal protocols were performed according to the Guidelines for Animal Experiments of the Kyushu University and of the Japanese Government.

Immunohistochemistry

The soleus muscles of all chloroquine-treated and untreated rats were excised and immediately frozen in isopentane cooled in liquid nitrogen. Six-micrometer serial sections cut on a cryostat were fixed in 4% paraformaldehyde at 4°C for 20 min. After endogenous peroxidase blocking with 0.3% H$_2$O$_2$, they were immersed in blocking solution containing 5% goat serum and 2% BSA in 0.01 M PBS at room temperature for 30 min, and incubated with the primary antibodies described later, diluted with 2% BSA in 0.01 M PBS at 4°C overnight. In addition, we used nonimmune rabbit serum or mouse IgG in the place of primary antibodies as negative controls. The next day, sections were incubated with biotinylated or FITC-labeled secondary antibodies at 37°C for 1 h. Then, sections were reacted with streptavidin-conjugated HRP and visualized with DAB, or examined by confocal laser microscopy. We also observed adjacent sections with H&E stain.

Western blotting

Total cellular protein was extracted from rat hind-limb muscles using a reducing sample buffer [10% SDS, 70 mM Tris–Hcl (pH 6.7), 5% β-mercaptoethanol, and 10 mM EDTA]. Protein concentrations were determined using the Bradford method. Twenty milligrams of protein per lane was separated by electrophoresis in 7–10% SDS polyacrylamide gels according to the molecular weights of the proteins recognized by the primary antibodies. The proteins were transferred to Immobilon PVDF membranes (Millipore, Bedford, MA) with an amperage of 5 mA/cm^2 for an hour. The blots were then incubated with the primary antibodies described later. Antibody binding was revealed by HRP-linked goat anti-rabbit or anti-mouse secondary antibodies and enhanced using chemiluminescence methods (Amersham Pharmacia, Biotech, UK).

Antibodies

The following primary antibodies were used for immuno-histochemistry: rabbit polyclonal anti-LC3 (1:100 dilution, MBL, Japan), anti-GRP78 (1:100, StressGen, Canada), anti-Aβ (1:400, Calbiochem Cat. No. NE1012, CA), and anti-caspase-12 (1:200, Chemicon, CA), and mouse monoclonal anti-sarcoplasmic or endoplasmic reticulum Ca2+ ATPase 2 (SERCA2, 1:500, Affinity BioReagents, CO), and anti-phosphorylated eukaryotic translation initiation factor-2α (eIF-2α, 1:100, Cell Signaling Technology, MA).

The following primary antibodies were also used in Western blotting experiments: rabbit polyclonal anti-LC3 (1:100, MBL), anti-Aβ (1:1000, Calbiochem Cat. No. NE1012), and anti-GRP78 (1:1000, StressGen), and mouse monoclonal anti-SERCA2 (1:2500, Affinity BioReagents).

The rabbit polyclonal anti-Aβ antibody used in this study is raised against a synthetic peptide corresponding to amino acids 3–16 of mouse and rat Aβ, and recognizes all isoforms of mouse and rat Aβ.

## Results

H&E staining

In the soleus muscles of rats treated with chloroquine for 3 weeks, type 1 fibers, which showed slightly denser staining than type 2 fibers, were mildly atrophic and had a somewhat granular appearance (Fig. 1a). After 5 weeks of treatment, most fibers became atrophic. Many of them had basophilic granular material in their sarcoplasm, and sev-

eral fibers showed rimmed vacuoles (Fig. 1d). In the muscles of rats treated with chloroquine for 7 weeks, almost all fibers contained basophilic granular material, and half of them had rimmed vacuoles (Fig. 1g). Several fibers were necrotic.

Immunohistochemistry

LC3 staining

In soleus muscles from normal control rats, most fibers showed no staining, except for several fibers with a faint granular appearance (not shown). In the muscles of rats treated with chloroquine for 3 weeks, almost all fibers showed granular staining in their sarcoplasm (Fig. 1b). In the muscles of rats treated with chloroquine for 5 weeks, in addition to sarcoplasmic granular staining, many vacuoles appeared in most type 1 and some type 2 fibers, the boundaries of which showed strong staining for LC3 (Fig. 1e). These vacuoles were not obvious in HE-stained sections. After 7 weeks of treatment, the number of vacuoles
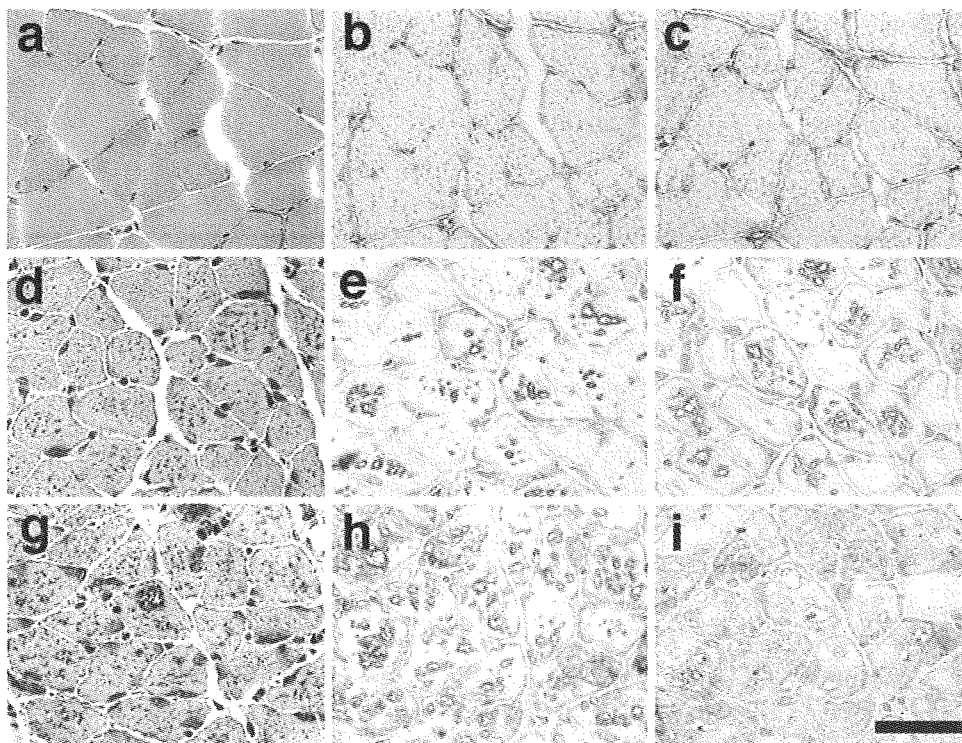
Fig. 1 Rimmed vacuole formation and localization of LC3 and SERCA2. **a–c** In soleus muscles from rats 3 weeks after the beginning of chloroquine treatment, type 1 fibers showed mild atrophy and a slightly granular appearance with H&E staining (**a**). LC3 (**b**) and SERCA2 (**c**) staining revealed a granular appearance in almost all fibers. **d–f** In muscles from rats treated with chloroquine for 5 weeks, many fibers had basophilic granular material in their sarcoplasm (**d**). LC3 (**e**) and SERCA2 (**f**) were strongly detected mainly around vacuoles, in addition to slight sarcoplasmic granular staining. **g–i** In muscles from rats treated with chloroquine for 7 weeks, almost all fibers contained basophilic granular material, and rimmed vacuoles became obvious with H&E staining (**g**). LC3 staining was intense around vacuoles (**h**). However, SERCA2 was no longer detected around vacuoles. Instead, most type 1 fibers showed faint sarcoplasmic staining. In several vacuoles, accumulations of SERCA2 positive materials were seen (**i**). **a, d**, and **g** H&E staining **b, e**, and **h** immunostaining for LC3. **c, f**, and **i** Immunostaining for SERCA2. **a–c, d–f**, and **g–i** show serial sections. *Bar* indicates 50 μm

increased, and their boundaries showed intense staining for LC3 (Fig. 1h).

SERCA2 staining

In soleus muscles from normal control rats, most type 1 fibers showed a faint granular appearance (not shown). In the muscles of rats treated with chloroquine for 3 weeks, most type 1 and some type 2 fibers showed granular staining in their sarcoplasm (Fig. 1c). In the muscles of rats treated with chloroquine for 5 weeks, most type 1 and some type 2 fibers had many vacuoles, the boundaries of which showed strong staining for SERCA2, similar to the LC3 staining pattern. Some of these fibers showed weak sarcoplasmic staining (Fig. 1f). After 7 weeks of treatment, however, there was no more staining around vacuoles than was seen at 5 weeks. Instead, most type 1 fibers showed faint sarcoplasmic staining. Moreover, there were accumulations of SERCA2-positive materials in several vacuoles (Fig. 1i).

Aβ staining

In soleus muscles from normal control rats, occasional granular staining was seen in several fibers (not shown). In the muscles of rats treated with chloroquine for 3 weeks, more than half of the fibers showed granular reactivity in their sarcoplasm (Fig. 2a). In the muscles of rats treated with chloroquine for 5 and 7 weeks, almost all fibers with vacuoles showed strong staining, especially around their vacuoles (Fig. 2b, c).

GRP78 staining

In soleus muscles from normal control rats and rats treated with chloroquine for 3 weeks, several fibers showed weak granular staining in their sarcoplasm (Fig. 3a). In the muscles of rats treated with chloroquine for 5 weeks, several fibers showed staining for GRP78 on the boundaries of vacuoles (Fig. 3b). After 7 weeks of treatment, almost half of the fibers with vacuoles showed GRP78 staining around rimmed vacuoles (Fig. 3c).

Phosphorylated eIF-2α staining

In soleus muscles from normal control rats and rats treated with chloroquine for 3 weeks, phosphorylation of eIF-2α was not confirmed (Fig. 3d). In the muscles of rats treated with chloroquine for 5 weeks, phosphorylation of eIF-2α was weakly detected around vacuoles in some fibers (Fig. 3e). After 7 weeks of treatment, several fibers with vacuoles were positively stained with anti-phosphorylated eIF-2α antibody around their vacuoles (Fig. 3f).

Caspase-12 staining

In soleus muscles from normal control rats and rats treated with chloroquine for 3 weeks, most fibers, with the exception of several fibers showing granular staining in their sarcoplasm, showed no staining for caspase-12 (Fig. 4a). In the muscles of rats treated with chloroquine for 5 weeks, fine granular staining was seen in the sarcoplasm of all fibers. Around vacuoles, caspase-12 showed slightly stronger staining than in the sarcoplasm (Fig. 4b). In rats treated with chloroquine for 7 weeks, intense and diffuse staining for caspase-12 was observed in all fibers (Fig. 4c).
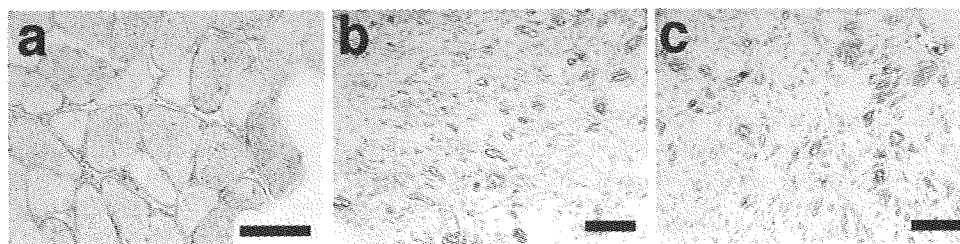
Western blotting (Fig. 5)

Aβ

Aβ levels began to increase after 3 weeks of treatment, and continued to increase thereafter.

LC3

We examined the conversion of cytosolic LC3-I (18 kDa) to membrane-associated LC3-II (16 kDa) by Western blotting analysis. In muscles from chloroquine-treated rats, LC3-II levels began to increase from 3 weeks after treatment.
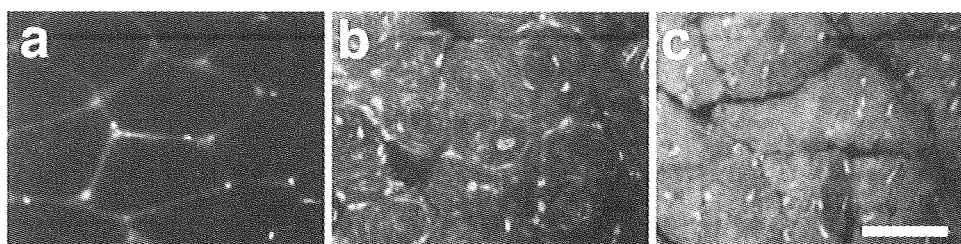

Fig. 2 Expression of Aβ protein. In soleus muscles from rats treated with chloroquine for 3 weeks, more than half of the fibers showed granular staining for Aβ (a). In the muscles of rats treated with chloro- quine for 5 (b) and 7 (c) weeks, almost all fibers with vacuoles showed strong staining for Aβ around their vacuoles. a–c Immunostaining for Aβ [40–42]. *Bars* indicate 50 μm
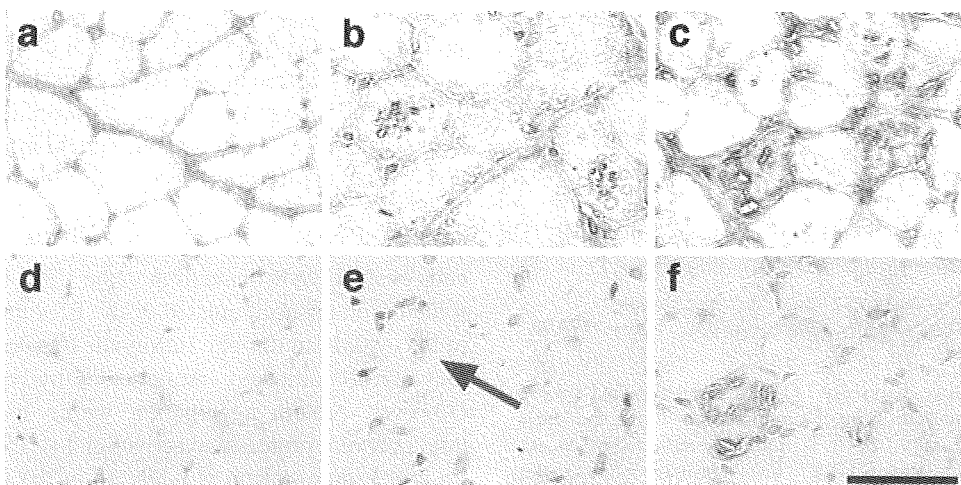
Fig. 3 Expression of GRP78 protein and phosphorylation of eIF-2α. In soleus muscles from rats treated with chloroquine for 3 weeks, GRP78 was faintly detected, showing a granular appearance in the sarcoplasm of several fibers (**a**) similar to the pattern in normal control rats (not shown). Phosphorylation of eIF-2α was not detected (**d**). In muscles from rats treated with chloroquine for 5 weeks, several fibers showed intense staining for GRP78 around their sarcoplasmic vacuoles (**b**). Phosphorylation of eIF-2αwas weakly detected around vacuoles in some fibers (*arrow*, **e**). In muscles from rats treated with chloroquine for 7 weeks, many fibers with rimmed vacuoles showed strong staining for GRP78 around vacuoles, in addition to weak sarcoplasmic staining (**c**). Phosphorylation of eIF-2α became obvious around vacuoles in several fibers (**f**). **a–c** Immunostaining for GRP78. **d–f** Immunostaining for phosphorylated eIF-2α. **a** and **d**, **b** and **e**, and, **c** and **f** show serial sections. *Bar* indicates 50 μm

Fig. 4 Expression of caspase-12 protein. In soleus muscles from rats treated with chloroquine for 3 weeks, caspase-12 was not detected, with the exception of some fibers with a small amount of faint granular staining (**a**). In muscles from rats treated with chloroquine for 5 weeks, almost all fibers showed staining for caspase-12, with a granular appearance (**b**). In muscles from rats treated with chloroquine for 7 weeks, almost all fibers showed diffuse and intense staining for caspase-12 in their sarcoplasm (**c**). **a–c** Immunostaining for caspase-12. *Bar* indicates 50 μm

GRP78

The levels of GRP78 were not increased in muscles from rats treated with chloroquine for 3 weeks compared with the levels in normal control rats. In the muscles of rats treated with chloroquine for 5 weeks, GRP78 levels began to increase; this increase continued until at least 7 weeks after the start of treatment.

SERCA2

Compared with normal control rats, SERCA2 levels were not significantly increased in muscles from rats treated with chloroquine for 3 weeks. In the muscles of rats treated with chloroquine for 5 weeks, SERCA2 levels were clearly increased. After 7 weeks of treatment, however, SERCA2 levels had decreased to the levels seen in normal control rats. These results support the findings obtained by immunohistochemistry.

Discussion

We demonstrated that chloroquine treatment induces Aβ accumulation, evokes ER stress, and finally activates autophagy in rat skeletal muscle.

LC3-II levels were increased by 3 weeks after the beginning of chloroquine treatment. LC3-II is degraded by lysosomal enzymes after the formation of autolysosomes, and the presence of lysosomal inhibitors causes the accumulation of LC3-II in autophagosomes and/or autolysosomes [23, 28, 38]. Therefore, this increased level of LC3-II is
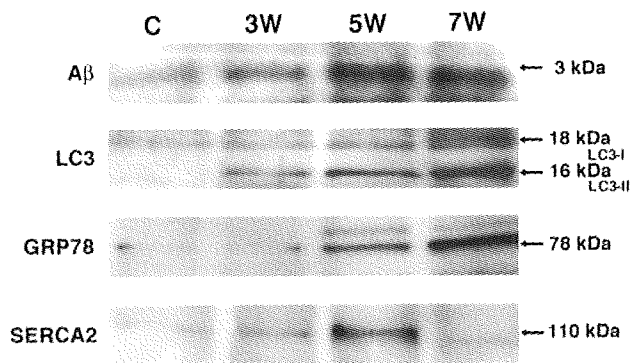
Fig. 5 Western blotting analysis of LC3, SERCA2, Aβ, and GRP78 levels. In hind-limb muscles from chloroquine-treated rats, the levels of Aβ and LC3, especially LC3-II, started to increase from 3 weeks after the beginning of treatment. GRP78 levels started to increase after 5 weeks. Note that the levels of SERCA2 were clearly increased by 5 weeks after the commencement of treatment; however, they were decreased by 7 weeks. Lanes C, 3W, 5W, and 7W represent control (untreated 5-week-old rats), and rats subjected to 3, 5 and 7 weeks of chloroquine treatment, respectively

probably caused by the disruption of lysosomal enzymes by the chloroquine treatment, rather than by the activation of autophagic activity itself. Moreover, Aβ accumulation was also detected at 3 weeks after the beginning of treatment. Taken together, these findings suggest that disruption of lysosomal enzymes and Aβ accumulation begin, at the latest, 3 weeks after the beginning of chloroquine treatment. It is not clear from this examination which process, disruption of lysosomal enzymes or accumulation of Aβ, takes place first. However, it has been recently reported that degradation of BACE, the β-secretase required for the generation of Aβ from APP, takes place in the lysosomal pathway and that chloroquine treatment inhibits BACE degradation, resulting in Aβ accumulaton [20]. Therefore, it is quite possible that in chloroquine-treated rats, lysosomal dysfunction leads to the Aβ accumulation.

The levels of GRP78 and caspase-12 began to increase 5 weeks after the commencement of treatment, and kept increasing thereafter. The phosphorylation of eIF-2α became visible 5 weeks after the beginning of treatment. Thus, an UPR owing to ER stress seems to be induced between 3 and 5 weeks after the beginning of treatment. The precise cause of this UPR induction is unclear. However, Aβ accumulation causes the disruption of Ca2+ homeostasis [9]. Dysregulation of intracellular Ca2+ is one major cause of ER stress [18, 26]. Therefore, Aβ accumulation might cause ER stress and induce an UPR in the muscles of chloroquine-treated animals. Indeed, Nakagawa et al. [31] showed that apoptotic cell death caused by Aβ overproduction is caused by ER stress and activation of caspase-12. In addition, ER stress and UPRs are detected in biopsies from IBM patients and cultured muscle fibers

overexpressing the gene for APP, which show colocalization of ER chaperones with Aβ, and co-immunoprecipitation of ER chaperones with APP, respectively [41].

On H&E staining, vacuolar degeneration was detected by 5 weeks after the beginning of chloroquine treatment, and became obvious by 7 weeks after the start of treatment. Therefore, it seems that autophagy activity is increased after the UPR is induced. Under conditions of ER stress, cells evoke ERAD in addition to the UPR: unfolded or misfolded proteins accumulated in the ER lumen are removed to the cytoplasm through retrograde translocation, and then they are ubiquitinated and degraded by proteasomes [27]. However, protein aggregation within the cytosol itself might prevent proteasome activation [4]. Indeed the ubiquitin-proteasome system is inhibited in the muscles of individuals with sporadic IBM [11]. Accordingly, it is possible that ERAD is disturbed in the muscles of chloroquine-treated rats. Recently, it was reported that autophagy is activated as a backup to ERAD if degradative substrates overwhelm the ERAD capacity [42], and that polyQ accumulation causes ER stress and then autophagy [21], although it remains controversial exactly which transducer is utilized for ER stress-induced autophagy in mammalian cells [32]. Therefore, it is possible that the activation of autophagy after ER stress induction also takes place to compensate for insufficient UPR and ERAD in the muscles of chloroquine-treated rats.

It is very interesting that, although the levels of SERCA2 increased as the UPR progressed, until 5 weeks after the initiation of treatment, they decreased later. In addition, some SERCA2 was located in vacuoles at 7 weeks after the start of treatment. In muscle cells, SERCA2 is thought to be mainly located in the sarcoplasmic reticulum (SR), a specialized form of smooth ER to handle Ca2+, rather than in the rough ER. Therefore, it is possible that this decline in the level of SERCA2 results from a decrease in the amount of SR membrane. Upon initiation of autophagy, autophagosomes are formed from the sequestration of cytoplasm and organelles by isolatior membranes. The origin of isolation membranes is still controversial [17]: they could be derived from the ER or assembled de novo at the site of their formation. It has been recently reported that yeast cells expand their ER volume under UPR-inducing conditions, that their ER membranes then form autophagosome-like structures to separate the ER filled with unfolded proteins, and that finally, their contents are degraded [5]. In addition, another recent report showed that the ER itself is engulfed by autophagosomes and is finally degraded [13]. Thus it is reasonable to suppose that, at first, the amount of membrane comprising the SR rather than the rough ER is increased to cope with the accumulation of unfolded proteins; however, the SR would gradually become saturated with unfolded proteins, and finally engulfed by autophagosomes and

degraded in skeletal muscle cells. The change in SERCA2 location from the vicinity of vacuoles into the vacuoles seems to support this hypothesis. Alternatively, skeletal muscle cells might attempt to exocytose the material in autophagosomes and/or autolysosomes following chloroquine treatment [24, 34].

In chloroquine-treated muscle, abnormality in autophagosomes formation is induced in type 1 fibers selectively [24, 37]. Therefore we examined the expression of SERCA2 protein. It is not clear why type 1 fibers are preferentially affected in chloroquine-treated muscle. Suzuki et al. [37] suggested that autophagy activity is higher in type 1 fibers than in type 2 fibers, because cellular lysosome predominantly exists in type 1 fibers. However, in sporadic IBM muscles, rimmed vacuoles are almost evenly distributed between type 1 and type 2 fibers, and the atrophic fibers are either type 1 or type 2. Further studies are needed to solve this problem.

Although we investigated the relationship between Aβ and ER stress, Aβ is known to disrupt mitochondrial function [7, 10]. Indeed, Aβ has been found in the mitochondria in both Alzheimer's disease brain [15] and the brains of transgenic mouse models of Alzheimer's disease overexpressing Aβ [8]. Moreover, mitochondrial abnormalities in sporadic IBM such as ragged-red fibers, cytochrome c oxidase-deficient fibers, and mitochondrial DNA deletions have been reported [3]. Therefore, there is a possibility that the pathogenic pathway via mitochondria is also involved in muscle fiber degeneration following chloroquine treatment.

In this study, we revealed that Aβ accumulation precedes the evocation of ER stress in rats treated with chloroquine. This is also true for other myopathies with rimmed vacuole formation [25]. Moreover, up-regulation of autophagy also took place in our rats. There have been many reports showing the activation of autophagy in skeletal muscle cells following chloroquine treatment [24, 37]. However, the mechanism underlying its activation seems to be more complex than it was previously thought: initial disruption of lysosomal enzymes by chloroquine leads to Aβ accumulation. Aβ accumulation causes ER stress, and finally autophagy becomes activated. Indeed, it has been reported that, in chloroquine-treated neurons, the activity of lysosomal enzymes becomes increased after the accumulation of autophagosomes and autolysosomes [6]. ER stress and up-regulation of autophagy have also been reported to be involved in the pathogenesis of Alzheimer's disease [40, 44]. Chloroquine-treated rats seem to be a useful model with which to investigate the pathogenesis of these diseases, especially from the viewpoint of the disturbance of protein quality control and degradation systems resulting from Aβ accumulation.

References

1. Askanas V, McFerrin J, Alvarez RB et al (1997) Beta APP gene transfer into cultured human muscle induces inclusion-body myositis aspects. Neuroreport 8:2155–2158
2. Askanas V, Engel WK (2001) Inclusion body myositis: newest concepts of pathogenesis and relation to aging and Alzheimer disease. J Neuropathol Exp Neurol 60:1–14
3. Askanas V, Engel WK (2008) Inclusion body myositis: muscle-fiber molecular pathology and possible pathogenic significance of its similarity to Alzheimer's and Parkinson's disease brains. Acta Neuropathol 116:583–595
4. Bence NF, Sampat RM, Kopito RR (2001) Impairment of the ubiquitin-proteasome system by protein aggregation. Science 292:1552–1555
5. Bernales S, Schuck S, Walter P (2007) ER-phagy: selective autophagy of the endoplasmic reticulum. Autophagy 3:285–287
6. Butler D, Brown QB, Chin DJ et al (2005) Cellular responses to protein accumulation involve autophagy and lysosomal enzyme activation. Rejuvenation Res 8:227–237
7. Cardoso SM, Santana I, Swerdlow RH et al (2004) Mitochondria dysfunction of Alzheimer's disease cybrids enhances Aβ toxicity. J Neurochem 89:1417–1426
8. Caspersen C, Wang N, Yao J et al (2005) Mitochondrial Aβ: a potential focal point for neuronal metabolic dysfunction in Alzheimer's disease. FASEB J 19:2040–2041
9. Christensen RA, Shtifman A, Allen PD et al (2004) Calcium dyshomeostasis in beta-amyloid and tau-bearing skeletal myotubes. J Biol Chem 279:53524–53532
10. Du H, Guo L, Fang F et al (2008) Cyclophilin D deficiency attenuates mitochondrial and neuronal perturbation and ameliorates learning and memory in Alzheimer's disease. Nat Med 14:1097–1105
11. Fratta P, Engel WK, McFerrin J et al (2005) Proteasome inhibition and aggresome formation in sporadic inclusion-body myositis and in amyloid-beta precursor protein-overexpressing cultured human muscle fibers. Am J Pathol 167:517–526
12. Fukuchi K, Pham D, Hart M et al (1998) Amyloid-beta deposition in skeletal muscle of transgenic mice: possible model of inclusion body myopathy. Am J Pathol 153:1687–1693
13. Hamasaki M, Noda T, Baba M et al (2005) Starvation on triggers the delivery of the endoplasmic reticulum to the vacuole via autophagy in yeast. Traffic 6:56–65
14. Hardy J, Selkoe DJ (2002) The amyloid hypothesis of Alzheimer's disease: progress and problems on the road to therapeutics. Science 297:353–356
15. Hirai K, Aliev G, Nunomura A et al (2001) Mitochondrial abnormalities in Alzheimer's disease. J Neurosci 21:3017–3023
16. Ikezoe K, Furuya H, Ohyagi Y et al (2003) Dysferlin expression in tubular aggregates: their possible relationship to endoplasmic reticulum stress. Acta Neuropathol 105:603–609
17. Juhasz G, Neufeld TP (2006) Autophagy: a forty-year search for a missing membrane source. PLoS Biol 4:e36
18. Kaufman RJ (1999) Stress signaling from the lumen of the endoplasmic reticulum: coordination of gene transcriptional and translational controls. Genes Dev 13:1211–1233
19. Kitazawa M, Green KN, Caccamo A et al (2006) Genetically augmenting Abeta42 levels in skeletal muscle exacerbates inclusion body myositis-like pathology and motor deficits in transgenic mice. Am J Pathol 168:1986–1997
20. Koh YH, von Arnim CA, Hyman BT et al (2005) BACE is degraded via the lysosomal pathway. J Biol Chem 280:32499–32504
21. Kouroku Y, Fujita E, Tanida I et al (2007) ER stress (PERK/eIF2alpha phosphorylation) mediates the polyglutamine-induced

LC3 conversion, an essential step for autophagy formation. Cell Death Differ 14:230–239

22. Levine B, Yuan J (2005) Autophagy in cell death: an innocent convict? J Clin Invest 115:2679–2688
23. Lünemann JD, Schmidt J, Schmid D et al (2007) β-amyloid is a substrate of autophagy in sporadic inclusion body myositis. Ann Neurol 61:476–483
24. Macdonald RD, Engel AG (1970) Experimental chloroquine myopathy. J Neuropathol Exp Neurol 29:479–499
25. Malicdan MC, Noguchi S, Nonaka I et al (2007) A Gne knockout mouse expressing human GNE D167 V mutation develops features similar to distal myopathy with rimmed vacuoles or hereditary inclusion body myopathy. Hum Mol Genet 16:2669–2682
26. Malhotra JD, Kaufman RJ (2007) The endoplasmic reticulum and the unfolded protein response. Semin Cell Dev Biol 18:716–731
27. Meusser B, Hirsch C, Jarasch E et al (2005) ERAD: the long road to destruction. Nat Cell Biol 7:766–772
28. Mizushima N, Yoshimori T (2007) How to interpret LC3 immunoblotting. Autophagy 3:542–545
29. Mori K (2000) Tripartite management of unfolded proteins in the endoplasmic reticulum. Cell 101:451–454
30. Nagaraju K, Casciola-Rosen L, Lundberg I et al (2005) Activation of the endoplasmic reticulum stress response in autoimmune myositis: potential role in muscle fiber damage and dysfuncton. Arthritis Rheum 52:1824–1835
31. Nakagawa T, Zhu H, Morishima N et al (2000) Caspase-12 mediates endoplasmic-reticulum-specific apoptosis and cytotoxicity by amyloid-beta. Nature 403:98–103
32. Ogata M, Hino S, Saito A et al (2006) Autophagy is activated for cell survival after endoplasmic reticulum stress. Mol Cell Biol 26:9220–9231
33. Pereira C, Ferreiro E, Cardoso SM et al (2004) Cell degeneration induced by amyloid-beta peptides: implications for Alzheimer's disease. J Mol Neurosci 23:97–104
34. Schmalbruch H (1980) The early changes in experimental myopathy induced by chloroquine and chlorphentermine. J Neuropathol Exp Neurol 39:65–81
35. Seglen PO, Berg TO, Blankson H et al (1996) Structural aspects of autophagy. Adv Exp Med Biol 389:103–111
36. Stauber WT, Hedge AM, Trout JJ et al (1981) Inhibition of lysosomal function in red and white skeletal muscles by chloroquine. Exp Neurol 71:295–306
37. Suzuki T, Nakagawa M, Yoshikawa A et al (2002) The first molecular evidence that autophagy relates rimmed vacuole formation in chloroquine myopathy. J Biochem (Tokyo) 131:647–651
38. Tanida I, Minematsu-Ikeguchi N, Ueno T et al (2005) Lysosomal turnover, but not a cellular level, of endogeneous LC3 is a marker for autophagy. Autophagy 1:84–91
39. Tsuzuki K, Fukatsu R, Takamaru Y et al (1995) Amyloid beta protein in rat soleus muscle in chloroquine-induced myopathy using end-specific antibodies for A beta 40 and A beta 42: immunohistochemical evidence for amyloid beta protein. Neurosci Lett 202:77–80
40. Unterberger U, Hoftberger R, Gelpi E et al (2006) Endoplasmic reticulum stress features are prominent in Alzheimer disease but not in prion diseases in vivo. J Neuropathol Exp Neurol 65:348–357
41. Vattemi G, Engel WK, McFerrin J et al (2004) Endoplasmic reticulum stress and unfolded protein response in inclusion body myositis muscle. Am J Pathol 164:1–7
42. Yorimitsu T, Nair U, Yang Z et al (2006) Endoplasmic reticulum stress triggers autophagy. J Biol Cell 281:30299–30304
43. Yoshida H, Matsui T, Yamamoto A et al (2001) XBP1 mRNA is induced by ATF6 and spliced by IRE1 in response to ER stress to produce a highly active transcription factor. Cell 107:881–891
44. Yu WH, Cuervo AM, Kumar A et al (2005) Macroautophagy—a novel beta-amyloid peptide generating pathway activated in Alzheimer's disease. J Cell Biol 171:87–98

Multiple system degeneration with basophilic inclusions in Japanese ALS patients with *FUS* mutation

Takahisa Tateishi · Toshihiro Hokonohara · Ryo Yamasaki · Shiro Miura ·
Hitoshi Kikuchi · Akiko Iwaki · Hiroshi Tashiro · Hirokazu Furuya ·
Yuko Nagara · Yasumasa Ohyagi · Nobuyuki Nukina · Toru Iwaki ·
Yasuyuki Fukumaki · Jun-ichi Kira

Abstract Mutations in the *fused in sarcoma* gene (*FUS*) were recently found in patients with familial amyotrophic lateral sclerosis (ALS). The present study aimed to clarify unique features of familial ALS caused by *FUS* mutation in the Japanese population. We carried out clinical, neuropathological, and genetic studies on a large Japanese pedigree with familial ALS. In six successive generations of this family, 16 individuals of both sexes were affected by progressive muscle atrophy and weakness, indicating an autosomal dominant trait. Neurological examination of six patients revealed an age at onset of 48.2 ± 8.1 years in fourth generation patients, while it was 31 and 20 years in fifth and sixth generation patients, respectively. Motor paralysis progressed rapidly in these patients, culminating in respiratory failure within 1 year. The missense mutation c.1561 C>T (p.R521C) was found in exon 15 of *FUS* in the four patients examined. Neuropathological study of one autopsied case with the *FUS* mutation revealed multiple system degeneration in addition to upper and lower motor neuron involvement: the globus pallidus, thalamus, substantia nigra, cerebellum, inferior olivary nucleus, solitary nucleus, intermediolateral horn, Clarke's column, Onuf's nucleus, central tegmental tract, medial lemniscus, medial longitudinal fasciculus, superior cerebellar peduncle, posterior column, and spinocerebellar tract were all degenerated. Argyrophilic and basophilic neuronal or glial cytoplasmic inclusions immunoreactive for FUS, GRP78/BiP, p62, and ubiquitin were detected in affected lesions. The *FUS* R521C mutation in this Japanese family caused familial ALS with pathological features of multiple system degeneration and neuronal basophilic inclusions.

Keywords Familial amyotrophic lateral sclerosis ·
Fused in sarcoma/translated in liposarcoma ·
Basophilic inclusion · Glial cytoplasmic inclusion

T. Tateishi · T. Hokonohara · R. Yamasaki · H. Kikuchi ·
Y. Nagara · Y. Ohyagi · J. Kira (✉)
Department of Neurology, Neurological Institute,
Graduate School of Medical Sciences, Kyushu University,
3-1-1 Maidashi, Higashi-ku, Fukuoka 812-8582, Japan
e-mail: kira@neuro.med.kyushu-u.ac.jp

H. Tashiro · T. Iwaki
Department of Neuropathology, Neurological Institute,
Graduate School of Medical Sciences, Kyushu University,
Fukuoka, Japan

T. Hokonohara · A. Iwaki · Y. Fukumaki
Division of Human Molecular Genetics,
Research Center for Genetic Information, Medical Institute
of Bioregulation, Kyushu University, Fukuoka, Japan

S. Miura
Division of Respirology, Neurology and Rheumatology,
Department of Medicine, Kurume University School
of Medicine, Kurume, Japan

H. Furuya
Department of Neurology, Neuro-Muscular Center,
National Omuta Hospital, Omuta, Japan

N. Nukina
Laboratory for Structural Neuropathology,
RIKEN Brain Science Institute, Wako, Saitama, Japan

Introduction

Amyotrophic lateral sclerosis (ALS) is a fatal neurodegenerative disorder characterized by a progressive loss of motor neurons. Approximately, 5–10% of cases are familial forms, which are usually transmitted by an autosomal dominant trait [30]. Genetically, 20–25% of familial ALS pedigrees have missense mutations in the *superoxide*

🌀 Springer

dismutase 1 gene (*SOD1*) [29], while *TARDBP* [10, 31], encoding TAR-DNA binding protein (TDP)-43, and *ANG* [7], encoding angiogenin, have also been linked to familial ALS. Recently, Kwiatkowski et al. [14] and Vance et al. [33] reported mutations in a gene encoding another DNA/RNA-binding protein called fused in sarcoma (FUS) specific for familial ALS. *FUS* mutations were detected in ~4% of familial ALS cases (~0.4% of all ALS cases) [15]. FUS is a nucleoprotein that functions in DNA and RNA metabolism [1, 2, 34, 35], and has been implicated in tumorigenesis [3, 28]. However, the precise roles of FUS have not been fully elucidated. Previous studies of *FUS*-mutation carriers revealed that the site of onset is the cervical region or proximal upper extremities, with subsequent spreading into the lower extremities; but neither bulbar signs nor cognitive deficits are apparent [14, 33]. Histologically, severe lower motor neuron loss in the spinal cord and, to a lesser degree, the brainstem, major pallor of the corticospinal tracts, mild to moderate upper motor neuron loss in the cerebral cortex, and mild myelin loss in the dorsal columns are observed, whereas dorsal horn neurons are unaffected [14, 33].

Herein, we report the clinical and pathological findings in a large Japanese familial ALS pedigree with an autosomal dominant inheritance pattern, and carrying a *FUS* R521C mutation. Patients demonstrated rapid progression of motor paralysis and pathological features of multiple system degeneration with argyrophilic and basophilic neuronal cytoplasmic inclusions and glial cytoplasmic inclusions containing FUS, revealing a unique phenotype of familial ALS caused by the *FUS* mutation.

Methods

### Patients and clinical study

This family came from the same identical district in Japan. In five successive generations, 16 individuals were affected by progressive muscle atrophy and weakness. Blood samples from 37 individuals, including four affected persons from the present family (Fig. 1a), were obtained with written informed consent. The patients were subjected to a thorough neurological examination. The clinical features of representative cases are described below.

Patient 1 (V-4)

The proband, whose parent died of ALS at 49 years of age, suffered from weakness of the right upper extremity from age 31 years. The patient was diagnosed with ALS by electromyography (EMG) and muscle biopsy at another hospital. The patient consulted our hospital 2 months after onset of weakness. Neurological examination disclosed muscle weakness, atrophy, and fasciculation in the right proximal upper limb, and hyperreflexia in the lower extremities. Subsequently, muscle weakness of the four extremities, gait disturbance, and dysphagia rapidly progressed, culminating in the patient being bedridden within 7 months. Sensory disturbance and cognitive impairment were not evident. The patient's respiratory function deteriorated and artificial ventilation was initiated 8 months after onset and continued for 14 years. Urinary disturbance and oculomotor paresis developed 4 years after onset and

Fig. 1 Pedigree tree of the present ALS family with *FUS* mutation and the mutation in *FUS* of patient 1. **a** *Filled symbols* indicate affected individuals. For confidentiality, gender and birth order are not shown. Five people in the pedigree were suspected to be asymptomatic carriers of a FUS mutation because their children with *FUS* mutations developed ALS, though their DNA samples were not available. **b** Direct sequencing shows a single base substitution (C1561T) in *FUS* of patient 1 (V-4). Antisense strands of *FUS* of patient 1 and a normal individual are shown
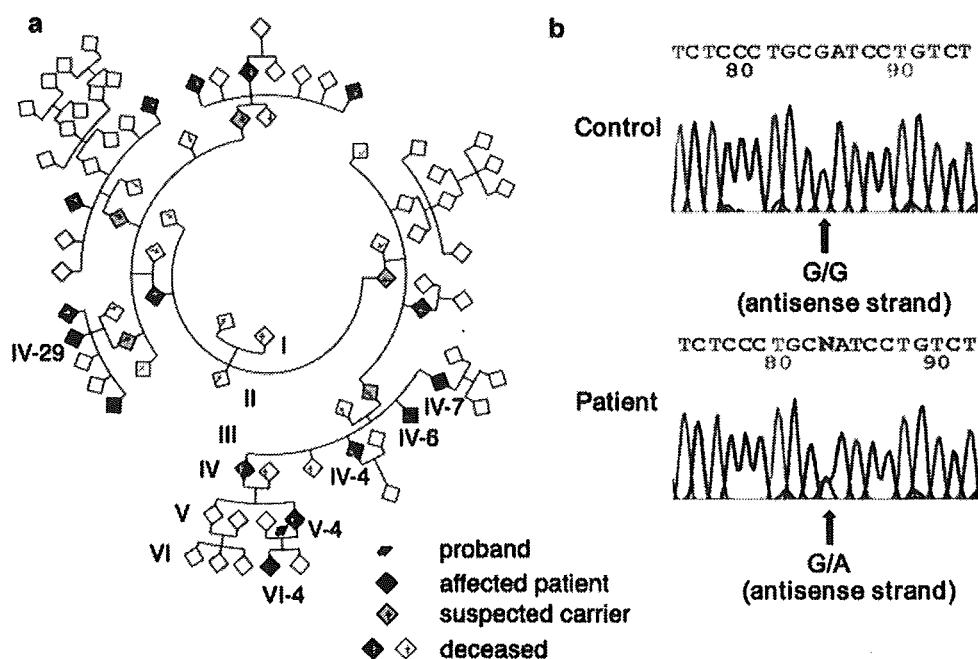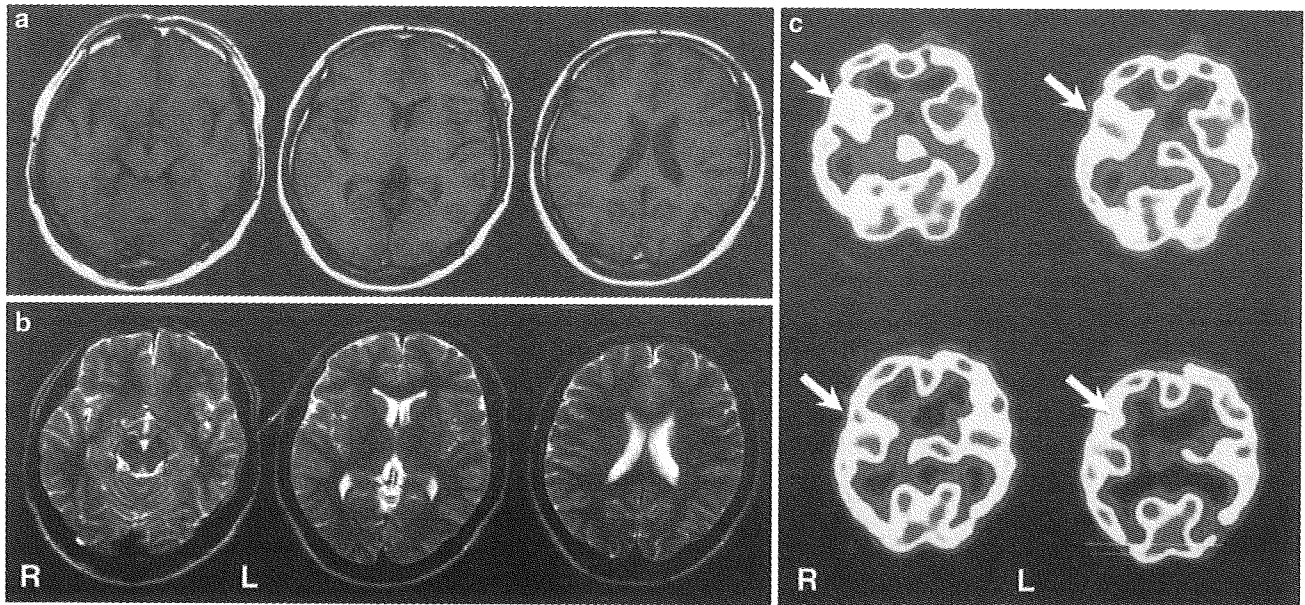
Fig. 2 Brain MRI and 99^mTc-ECD SPECT of patient 2 on admission obtained 6 months after onset. **a** T1- (TE 14.0/TR 585.0) and **b** T2-weighted axial images (TE 96.0/TR 3203.0) demonstrate no abnormality. **c** SPECT findings show a decrease in cerebral blood flow in the right striatum, thalamus, and fronto-temporal lobe (*arrows*)

the patient died from hemorrhagic shock at the age of 45 years. Total disease duration was 14 years.

Patient 2 (VI-4)

The patient, a child of patient 1, suffered from weakness of bilateral upper limbs from age 20 years. For the 2 months following onset, bilateral arm weakness progressively worsened and the patient experienced difficulty with running. The patient was admitted to our hospital 6 months after onset. Neurological examination revealed moderate muscle weakness and atrophy of the bilateral trapezius and sternocleidomastoid muscles, with sparing of the cranial nerves innervating other muscles. The patient had a proximal dominant severe weakness, atrophy, and fasciculation in the bilateral upper limb muscles. Mild hyperreflexia and mild muscle weakness without atrophy were also noted in both lower limbs. The plantar response was flexor. Neither cognitive impairment nor sensory disturbance was observed. No abnormal findings were found in serum laboratory tests, except for mild elevation of creatine kinase to 598 U/l (normal range: 62–287). The results of CSF examination were normal. EMG showed chronic neurogenic patterns, including giant motor unit potentials in the right biceps, deltoid, first dorsal interossei, and anterior tibial muscles. The results of nerve conduction tests were essentially normal, except for a slightly prolonged F-wave latency in the left peroneal nerve. Motor-evoked potentials elicited by stimulation of the median nerve showed prolonged peripheral latency and normal central conduction

time bilaterally, while those elicited by stimulation of the posterior tibial nerve were normal. Somatosensory-evoked potential studies were normal. Brain and cervical spinal cord MRI findings were normal, while a 99mTc-ethylcysteinate dimer SPECT (99mTc-ECD SPECT) study showed a decrease in cerebral blood flow in the right striatum, thalamus, and fronto-temporal lobe (Fig. 2). There was no mutation in *SOD1*. Nine months after onset, mechanical ventilation was introduced because of respiratory failure. Disease duration at the last examination was 14 months.

Patient 3 (IV-7)

This patient noticed muscle weakness of the right foot and left arm at age 51 years and was diagnosed with ALS at another hospital using electrophysiological tests including EMG. Weakness in both arms progressively worsened. Dysphagia and dysarthria appeared 6 months after onset. Neurological examination at 8 months after onset showed dysarthria, dysphagia, tongue atrophy, neck weakness and proximal dominant muscle weakness, and atrophy of the bilateral upper limbs. Spasticity, hyperreflexia, and extensor plantar response were noted in the left lower limb. After one year, the respiratory disturbance became worse, resulting in death at age 52. Total disease duration was 21 months.

Patient 4 (IV-29)

At 58 years of age, this patient suffered from left leg weakness that progressively deteriorated during the

following 8 months. Neurological examination demonstrated muscle weakness, fasciculation, and atrophy of the left lower limb and hyperreflexia in both the lower limbs. No sensory disturbance was noted. EMG findings showed chronic neurogenic patterns. Muscle weakness spread to both the upper limbs and the patient could not raise the arms. The gait disturbance progressed, and the patient was unable to walk unaided at 19 months after onset. Dysphagia and dysarthria appeared thereafter. Muscle weakness of all four extremities progressed rapidly and the patient was bedridden at 22 months after onset. Respiratory dysfunction became overt at 25 months after onset and the patient started mechanical ventilation at 26 months after onset. The disease duration at the last examination was 7 years.

Neuropathological study

A postmortem examination of patient 1 was performed 17 h after death. Brain and spinal cord specimens were fixed for 2 weeks in buffered 10% formalin, embedded in paraffin, and then sliced into 6-μm-thick sections. The sections were stained with hematoxylin and eosin (HE), Bodian, and Gallyas stains. We tested three anti-FUS antibodies, each of which recognizes a different epitope. Anti-FUS rabbit polyclonal antibody (Ab–TLS–M) was provided by the Laboratory for Structural Neuropathology and the Research Resource Center, RIKEN Brain Science Institute [4]. The anti-FUS antibodies were generated against a peptide encompassing amino acids 260–274 of mouse FUS. Anti-FUS rabbit polyclonal antibodies made by Bethyl Laboratories (Montgomery, TX, USA) and Novus Biologicals (Littleton, CO, USA) recognize an N-terminal epitope, encompassing amino acids 1–50 of human FUS. Immunohistochemistry experiments using these three antibodies revealed equally labeled cytoplasmic inclusions. Therefore, the polyclonal antibody Ab-TLS-M was used for all subsequent immunostaining experiments. The following primary antibodies and dilutions were used for immunohistochemical investigations: anti-FUS rabbit polyclonal antibody (Ab-TLS-M) (1:500) [4], anti-FUS rabbit polyclonal antibody (1:250, Bethyl Laboratories), anti-FUS rabbit polyclonal antibody (1:250, Novus Biologicals), anti-ubiquitin rabbit polyclonal antibody (1:500, DAKO, Glostrup, Denmark), anti-p62 rabbit polyclonal antibody (1:1,000, Biomol, Plymouth Meeting, PA, USA), anti-78-kDa glucose-regulated protein/immunoglobulin heavy-chain binding protein (GRP78/BiP) rabbit polyclonal antibody (1:500, Santa Cruz, Santa Cruz, CA, USA), anti-microtubule-associated protein (MAP)-2 mouse monoclonal antibody (1:500, clone HM-2, Sigma, Saint Luis, MO, USA), anti-phosphorylated neurofilament mouse monoclonal antibody (1:500, clone

2F11, DAKO, Glostrup, Denmark), anti-SOD1 sheep polyclonal antibody (1:500, Binding Site, Birmingham, UK), anti-tau rabbit polyclonal antibody (1:500, DAKO, Glostrup, Denmark), anti-β-actin mouse monoclonal antibody (1:500, clone AC-15, Sigma, Saint Luis, MO, USA), anti-α-synuclein mouse monoclonal antibody (1:500, clone Sf38, Santa Cruz, Santa Cruz, CA, USA), anti-αB-crystallin rabbit polyclonal antibody (1:500) [9], anti-cystatin C rabbit polyclonal antibody (1:1,000, DAKO, Glostrup, Denmark), anti-polyglutamine mouse monoclonal antibody (1:500, clone 2c11, Millipore, Billerica, MA, USA), and anti-TDP43 rabbit polyclonal antibody (1:10,000, Cosmo Bio, Tokyo, Japan). The secondary antibodies were horseradish peroxidase-conjugated anti-rabbit antibody (PI-1000) and horseradish peroxidase-conjugated anti-mouse antibody (PI-2000) (1:500, both from Vector Laboratories, Burlingame, CA, USA). Immunohistochemistry was also performed using an indirect immunoperoxidase method as previously described [11]. The sections were deparaffinized in xylene, dehydrated in ethanol, and then incubated with 0.3% hydrogen peroxide in absolute methanol for 30 min at room temperature to inhibit endogenous peroxidase activity. After rinsing in tap water, the sections were completely immersed in distilled water and then heated in 0.01 M citrate buffer (pH 6.0) in a microwave for 10 min for antigen retrieval. After this pretreatment, the sections were incubated with a primary antibody diluted in 5% normal goat serum in 20 mM Tris–HCl (pH 7.6) containing 0.5 M NaCl, 0.05% NaN₃, and 0.05% Tween 20 (TBST) at 4°C overnight, and then with a 1:200 dilution of the appropriate secondary antibody for 1 h at room temperature. A colored reaction product was developed using 3,3′-diaminobenzidine tetrahydrochloride (DAB) solution (0.02% DAB, 0.003% H₂O₂, 50 mM Tris–HCl, pH 7.6). The sections were lightly counter-stained with hematoxylin. Neuronal and glial cytoplasmic inclusions immunoreactive for FUS were evaluated using a semi-quantitative grading system, similar to the one used in a previous study [22] in which pathological lesions were scored as none (−), rare (+), occasional (++), common (+++), or numerous (++++).

Genetic analysis

We performed genetic analysis for FUS mutations using peripheral blood samples obtained from the four patients. Exons 5, 6, 14, and 15 of FUS were amplified by polymerase chain reaction (PCR) using intronic primers [14, 33]. The PCR product was sequenced using a Big-Dye Terminator Sequencing Kit (Applied Biosystems). Sequencing reactions were performed using an automated Applied Biosystems Model 3100 DNA sequencer.

Results

Clinical findings

The clinical features are summarized in the Table 1. The family history suggests an autosomal dominant inheritance pattern. Both sexes (11 men and 5 women) were affected. Mean age at onset was 40.6 ± 13.8 years ($n = 6$, mean ± SD), and mean duration from onset to respiratory failure was 11.7 ± 7.3 months ($n = 6$, mean ± SD). Age at onset in the fourth generation was 48.2 ± 8.1 years ($n = 4$, mean ± SD) while it was 31 and 20 years in the fifth ($n = 1$) and sixth ($n = 1$) generations, respectively. Three out of six patients examined, showed preferential involvement of the proximal upper extremities with flailing arms and subsequent spread of motor weakness to the lower extremities.

General autopsy findings in patient 1

General autopsy examinations demonstrated bronchopneumonia with bilateral pulmonary edema in the upper lobes and pulmonary atelectasis in the right lower lobe. There was also unclotted blood in the small intestine and colon lumen. However, the origin of the bleeding in the gastrointestinal tract was not clear.

Neuropathological findings in patient 1

The patient's brain weighed 1,070 g at autopsy. A macroscopic examination demonstrated severe atrophy of the bilateral frontal lobes, brainstem, cerebellum, and spinal cord (Fig. 3a–c). Bilateral precentral gyri were mildly atrophic. Anterior roots of spinal nerves were markedly atrophied, while posterior roots were moderately atrophic (Fig. 3d, e). By Klüver–Barrera staining, severe degeneration was found in the central tegmental tracts, medial lemniscus, medial longitudinal fasciculus, superior cerebellar peduncles, lateral corticospinal tracts, posterior columns, and spinocerebellar tracts. Neurons were markedly lost from the anterior horns, intermediolateral horns, Clarke's columns, and Onuf's nuclei in the spinal cord (Fig. 4a–c). Ganglion cells also disappeared from the dorsal root ganglia. Moreover, severe neuronal loss was seen in the Betz cells of the primary motor cortex, the inner and outer segments of the global pallidus, the thalami, compact and reticular parts of the substantia nigra, the Purkinje and granular cells and dentate nucleus of the cerebellum, the trochlear and abducens nuclei of the midbrain, and the inferior olivary, hypoglossal, ambiguous, and solitary nuclei of the medulla oblongata (Fig. 4d). All of these nerve cell losses were associated with heavy astrogliosis as determined by GFAP immunostaining and

Table 1 Clinical features of ALS patients in the present family

	Patient 1 V-4	Patient 2 VI-4	Patient 3 IV-7	Patient 4 IV-29	Patient 5 IV-6	Patient 6 IV-4
Age at onset (years)	31	20	51	58	45	39
Age at death (years)	45	NA	52	NA	46	42
Initial symptoms	Weakness of right upper limb	Weakness of bilateral upper limbs	Weakness of right upper and lower limbs	Weakness of left lower limbs	Weakness of bilateral upper limbs	Gait disturbance
Weakness and atrophy at onset						
Upper limbs	Prox > dist	Prox > dist	Prox > dist	Almost normal	Affected	Affected
Lower limbs	Almost normal	Prox > dist	Almost normal	Prox > dist	Almost normal	Affected
Respiratory muscle	−	+	−	+	Unknown	Unknown
Cranial nerve	−	−	+	+	Unknown	Unknown
Duration from onset to respiratory failure	9 months	9 months	1 year	1 year	25 months	3 years
Mechanical ventilation	+	+	−	+	−	−

Patients 1–4 have the *FUS* mutation. DNA samples from patients 5 and 6 were not available

NA not applicable, *prox* proximal, *dist* distal
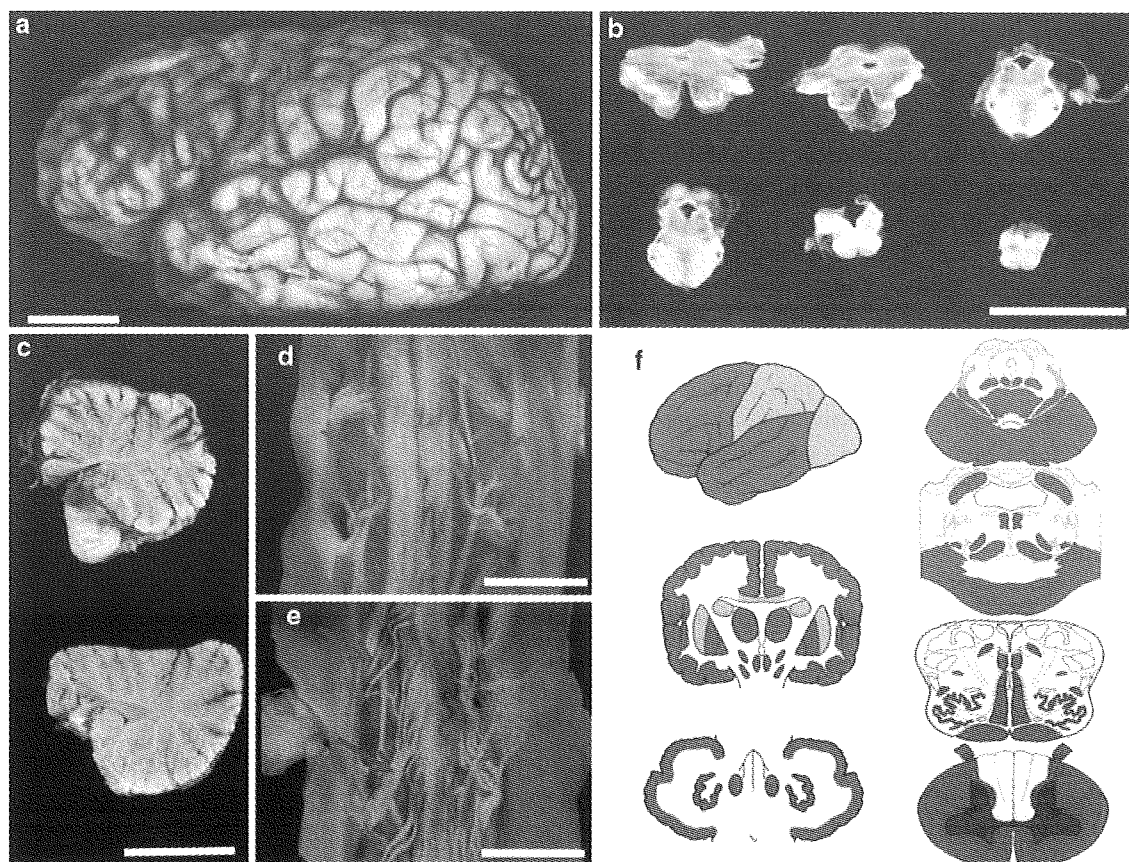
Fig. 3 Macroscopic findings in patient 1. Macroscopically, bilateral frontal lobes (**a**), brainstem (**b**), cerebellum (**c**), and spinal cord (**d, e**) show severe atrophy. Anterior roots of the spinal nerves in front view (**d**, *arrows*) are markedly atrophic while posterior roots in back view (**e**, *arrows*) also show moderate atrophy. **f** Schematic illustrations indicating the distribution of degeneration based on HE staining and gross findings in the CNS of patient 1. Colors indicate grades of involvement as mild (*green*), moderate (*yellow*), and severe (*red*) in each region examined based on HE staining and gross findings. *Scale bars* 3 cm (**a–c**), and 1 cm (**d–e**)

Holzer staining. The hippocampi and parahippocampal gyri were not atrophic, and pyramidal cells in the hippocampi were not lost. Argyrophilic and basophilic neuronal cytoplasmic inclusions were often seen in oculomotor, pontine, and Meynert nuclei, and these were immunoreactive for FUS, ubiquitin, p62, and GRP78/BiP, but not for MAP-2, phosphorylated neurofilament, SOD1, Tau, β-actin, α-synuclein, αB-crystallin, cystatin C, polyglutamine, or TDP43 (Fig. 4e–k). Following HE staining, the basophilic neuronal cytoplasmic inclusions showed an eosinophilic core with HE staining, which was surrounded by a pale basophilic halo similar to those described in a previous report [6]. Additionally, glial cytoplasmic inclusions were revealed by FUS immunostaining (Fig. 4l–n). FUS-immunoreactive glial cytoplasmic inclusions were also immunopositive for ubiquitin and p62, and appeared to extend into the radiating processes. Lewy bodies were not detected, and neither Tau nor α-synuclein immunoreactivity was found in glial cytoplasmic inclusions. No ubiquitinated neuronal inclusions were observed either in the hippocampus or in the cerebral cortex. In all brain and spinal cord regions, FUS-positive neuronal and glial inclusions were more frequently and widely observed than basophilic, ubiquitin-, and silver-positive inclusions (Table 2). Neurons were markedly missing from the anterior horns. Glial cytoplasmic inclusions were detected in the anterior horns, but not neuronal cytoplasmic inclusions. FUS-positive glial inclusion bodies were diffuse in the white matter, but demyelinating lesions were not detected. In the controls, FUS immunoreactivity was more strongly detected in the neuronal nuclei of the anterior horn cells relative to that in the neuronal cytoplasm (Fig. 4r). In patient 1, in neurons without inclusion bodies, faint diffuse nuclear immunostaining to FUS with prominent nucleolar staining was seen, while such FUS nuclear staining was not apparent in neurons without inclusions (Fig. 4k).

Genotype findings

Mutations in the *FUS* gene have previously been identified in familial ALS cases [14, 33]. Therefore, we conducted mutation scanning of exons 5, 6, 14, and 15 of *FUS* by
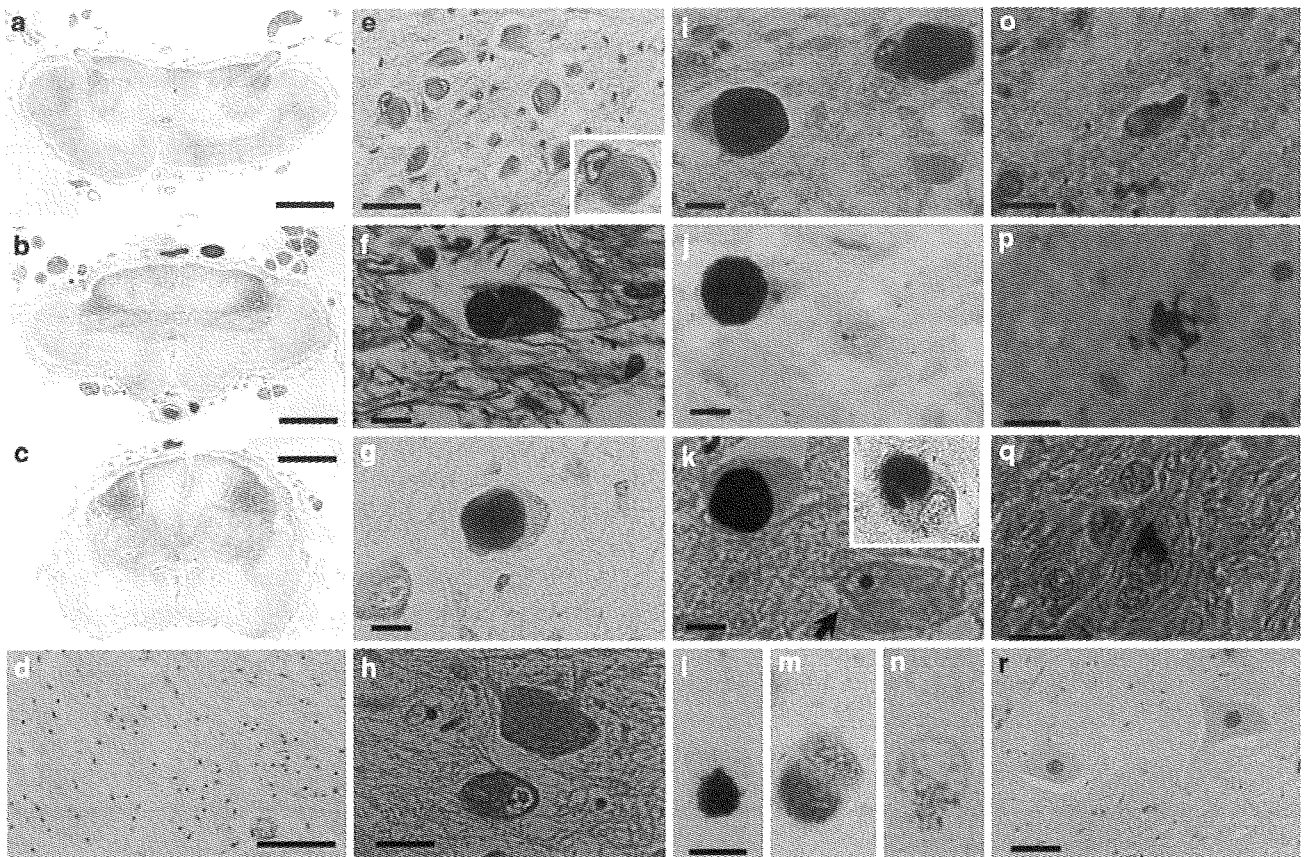
Fig. 4 Microscopic findings in patient 1. a–c Klüver–Barrera (KB) staining of axial sections of the spinal cord shows severe degeneration of bilateral lateral corticospinal tracts and posterior columns in the cervical (a), thoracic (b), and lumbar cord (c). d HE staining shows severe neuronal loss with neuropil rarefaction in the anterior horns of the lumbar cord. e HE staining shows basophilic neuronal cytoplasmic inclusions in the oculomotor nucleus. The basophilic neuronal cytoplasmic inclusions are stained with Bodian (f) and Gallyas stains (g). GRP78/BiP (h), ubiquitin (i), p62 (j), and FUS (k) immunoreactivities can be seen in cytoplasmic inclusions in the oculomotor nucleus. Faint diffuse nuclear immunostaining to FUS with prominent nucleolar staining is present in the adjacent neuron without the inclusion (arrow in k), while FUS nuclear staining is not apparent in the red nucleus with a FUS inclusion on the same section (inset in k). j and k are consecutive sections. FUS (l), ubiquitin (m), and GRP78/BiP (n) immunoreactivities are seen in cytoplasmic inclusions in the precentral gyrus. These images (l–n) are of consecutive sections. Glial cytoplasmic inclusions immunoreactive for ubiquitin (o), p62 (p), and FUS (q) can be seen in the cerebral peduncle. Staining of the anterior horn cells of a control individual demonstrates diffuse nuclear staining without inclusions (r). Scale bars 2 mm (a–c), 100 μm (d), 50 μm (e), 10 μm (f–q), and 50 μm (r)

direct sequencing, and found a missense mutation, 1561 C>T (R521C), within exon 15 of FUS in four affected family members (patients 1–4) (Fig. 1b). This missense mutation is identical to one of the FUS mutations previously reported [14, 33]. DNA specimens from the other two patients who were clinically examined (patients 5 and 6) were not available. We also found that 2 of 34 non-affected individuals tested were heterozygous for the relevant mutation.

Discussion

In the present study, we describe the first Japanese family with ALS with the FUS R521C mutation that is one of the most common mutations of the gene located in the highly conserved C-terminus region. Thus, FUS mutation should be considered as one of the causes of familial ALS in Japanese populations.

Average age at onset is reported as around 45 years and average survival is about 33 months after onset [14, 33]. In our patients, average age at onset in the fourth generation was comparable to those reported previously; however, patients in the fifth and sixth generations had average ages at onset that were 20 and 30 years, respectively, earlier than that in the fourth generation patients and showed very rapid progression culminating in respiratory failure within 9 months of onset. Genetic anticipation is usually seen in trinucleotide repeat disorders, but not in the case of missense mutations. Thus, factors other than the FUS mutation may have contributed to the accelerated onset and very rapid progression in the descendant generations of this

Table 2 Semiquantitative grading of neuronal and glial cytoplasmic inclusions immunoreactive for FUS in different anatomical regions

Anatomical region	FUS-positive NCI	FUS-positive GCI
Frontal cortex	++++	+++
Temporal cortex	++++	+++
Parietal cortex	++++	+++
Occipital cortex	++	++
Hippocampus—dentate	++++	+++
Hippocampus—CA1	++++	+++
Corpus callosum	-	+++
Thalamus	++++	+++
Oculomotor nuclei	++++	-
Substantia nigra	+++	+++
Pontine nuclei	++++	+++
Spinal cord—ventral gray	-	++
Cerebellum—cortex	-	-
Cerebellum-white matter	++++	++++

Semiquantitative grading: − none, + rare, ++ occasional, +++ common, and ++++ numerous

NCI neuronal cytoplasmic inclusion, *GCI* glial cytoplasmic inclusion

family. Alternatively, this may be a chance effect. Preferential onset in upper limbs, as found in the family reported here, has also been described in families with *FUS* mutations [14, 33]. Thus, onset in the proximal upper limbs with subsequent spreading to the lower limbs appears to be a characteristic feature of familial ALS caused by *FUS* mutation, irrespective of race.

Interestingly, the autopsied case, whose disease duration was 13 years with mechanical ventilation, showed multiple system degeneration in addition to upper and lower motor neuron involvements: neurons in the inner and outer segments of the globus pallidus, thalami, compact and reticular parts of substantia nigra, Purkinje and granular cells and dentate nucleus of the cerebellum, inferior olivary nucleus, solitary nucleus, intermediolateral horns, Clarke's columns, and Onuf's nucleus were lost, and the central tegmental tracts, medial lemniscus, medial longitudinal fasciculus, superior cerebellar peduncles, posterior columns, and spinocerebellar tracts showed degeneration. The pathology of the autopsied materials demonstrated extensive cerebellar atrophy, probably because 14 years had passed since onset. Cerebellar ataxia was not apparent clinically before initiating artificial ventilation within a year of disease onset. We could not evaluate whether cerebellar symptoms developed clinically in the patient after initiating artificial ventilation, because of severe weakness of the four limbs. In previous reports, the only extra-motor involvement found has been mild myelin loss in the dorsal columns [33]. The occurrence of widespread neurodegeneration involving multiple systems, may be related to the long disease duration in our patient. For example, sporadic ALS cases in a totally locked-in state show widespread degeneration beyond the motor neuron system [8, 17]. However, widespread degeneration is not always a feature in sporadic ALS patients surviving for long periods with respiratory assistance [24, 27, 36]. In addition, Nishihira et al. [24] reported that the distribution patterns of TDP-43-immunoreactive neuronal cytoplasmic inclusions were not influenced by long-term survival with artificial respiratory support. In patient 2, a decrease in cerebral blood flow in the right striatum, thalamus, and fronto-temporal lobe was evident in the very early course of the disease. We assumed that subclinical neural dysfunction in multiple systems started in the early course of the disease, resulting in widespread neurodegeneration of multiple systems in the late stage of *FUS* mutation-related ALS.

The present autopsied case showed basophilic neuronal cytoplasmic inclusions in oculomotor nuclei, pontine nuclei, and Meynert nuclei. Perhaps, as anterior horn cells in the spinal cord showed a remarkable disappearance, no basophilic inclusions were seen in the anterior horns. Basophilic inclusions were distributed in regions, where neurons were relatively preserved. The presence of FUS-positive cytoplasmic inclusions that were immunopositive for ubiquitin and p62 in the anterior horn neurons has been described [33]. The inclusions in our case were positive for FUS, ubiquitin, p62, and GRP78/BiP, but not for MAP-2, phosphorylated neurofilament, SOD1, Tau, β-actin, α-synuclein, αB-crystallin, cystatin C, or polyglutamine, suggesting a distinct mechanism from those underlying the formation of Lewy bodies, Bunina bodies, and neurofibrillary tangles. Although neuronal basophilic inclusions are rarely observed in the spectrum of motor neuron diseases, such as juvenile ALS [16, 20, 26], adult-onset ALS [12, 13], frontal lobe syndrome [19], and familial ALS with posterior column involvement [32], these inclusions are negative for ubiquitin and are therefore different from those found in patients with *FUS* mutation-related ALS. The presence of ubiquitin and GRP78/BiP in FUS-positive inclusions indicates an involvement of protein misfolding and endoplasmic reticulum stress. In patients with the *FUS* mutation, aberrant cytoplasmic localization and an increase in the level of total insoluble FUS is reported [14, 33]. Doi et al. [4] reported that FUS is a major nuclear aggregate-interacting protein in a model of Huntington's disease [4]. However, in Huntington's disease, FUS protein shifts into nuclear aggregates with polyglutamine in neurons [4]. In contrast, in this familial ALS case, FUS protein aggregates were present in the neuronal cytoplasm. FUS-positive neuronal and glial inclusions were found more frequently and widely than basophilic, ubiquitin-, and silver-positive inclusions in all brain and spinal regions. Thus, it was

assumed that ubiquitination of FUS is a late event. Therefore, mislocalization of nuclear protein and the presence of cytoplasmic aggregates are similar to the findings in familial ALS patients with mutations in *TARDBP*, suggesting that both conditions have similar pathogenic mechanisms.

In our cases, FUS-positive inclusions were seen in the glial cytoplasm as well as in neuronal cytoplasm. Multiple system degeneration involving the fronto-temporal cortex, hippocampal formation, neostriatum, and substantia nigra is observed in sporadic ALS cases with long disease duration and on artificial ventilation. In such cases, TDP-43-immunoreactive neuronal and glial cytoplasmic inclusions are widespread in the central nervous system [23, 24]. Neumann et al. [21] found that FUS-labeled ubiquitin-positive neuronal and glial cytoplasmic inclusions are seen in fronto-temporal lobar degeneration (FTLD), with the neuronal inclusions composed of an unidentified ubiquitinated protein (FTLD-U). In addition, abundant FUS immunoreactivity can be found in inter-mediate filament inclusion disease (NIFID), presenting as FTLD [22]. Recently, Munoz et al. [18] reported FUS pathology in basophilic inclusion body disease, a tau-negative form of FTLD. Inclusion bodies found under these conditions do not contain TDP-43 [18, 21, 22]. Accordingly, Frank and Tolnay [5] proposed that FTLD-U, NIFID, and BIDB can be referred to as FUS protein-opathies (FTLD-FUS). FUS may thus contribute to the development of FTLD and ALS with multiple system degeneration as TDP-43 does. However, distinct molecu-lar pathways may be involved because the protein structures of FUS and TDP-43 are different. In TDP-43 proteinopathy, truncated TDP-43 with a deletion of the C-terminal part has a primary role in the formation of inclusions, leading to neuronal degeneration [25]. In this study we did not evaluate whether truncations in FUS might occur, similar to those described for TDP-43. Therefore, we think determining the existence of such a truncation in FUS would be an interesting future study.

References

1. Baechtold H, Kuroda M, Sok J, Ron D, Lopez BS, Akhmedov AT (1999) Human 75-kDa DNA-pairing protein is identical to the pro-oncoprotein TLS/FUS and is able to promote D-loop for-mation. J Biol Chem 274:34337–34342
2. Bertrand P, Akhmedov AT, Delacote F, Durrbach A, Lopez BS (1999) Human POMp75 is identified as the pro-oncoprotein TLS/FUS: both POMp75 and POMp100 DNA homologous pairing activities are associated to cell proliferation. Oncogene 18:4515–4521
3. Crozat A, Aman P, Mandahl N, Ron D (1993) Fusion of CHOP to a novel RNA-binding protein in human myxoid liposarcoma. Nature 363:640–644
4. Doi H, Okamura K, Bauer PO et al (2008) RNA-binding protein TLS is a major nuclear aggregate-interacting protein in Huntingtin exon 1 with expanded polyglutamine-expressing cells. J Biol Chem 283:6489–6500
5. Frank S, Tolnay M (2009) Frontotemporal lobar degeneration: toward the end of conFUSion. Acta Neuropathol 118:629–631
6. Fujita K, Ito H, Nakano S, Kinoshita Y, Wate R, Kusaka H (2008) Immunohistochemical identification of messenger RNA-related proteins in basophilic inclusions of adult-onset atypical motor neuron disease. Acta Neuropathol 116:439–445
7. Greenway MJ, Andersen PM, Russ C et al (2006) ANG mutations segregate with familial and 'sporadic' amyotrophic lateral scle-rosis. Nat Genet 38:411–413
8. Hayashi H, Kato S (1989) Total manifestations of amyotrophic lateral sclerosis. ALS in the totally locked-in state. J Neurol Sci 93:19–35
9. Iwaki T, Kume-Iwaki A, Liem RK, Goldman JE (1989) Alpha B-crystallin is expressed in non-lenticular tissues and accumulates in Alexander's disease brain. Cell 57:71–78
10. Kabashi E, Valdmanis PN, Dion P et al (2008) TARDBP muta-tions in individuals with sporadic and familial amyotrophic lateral sclerosis. Nat Genet 40:572–574
11. Kikuchi H, Doh-ura K, Kawashima T, Kira J, Iwaki T (1999) Immunohistochemical analysis of spinal cord lesions in amyo-trophic lateral sclerosis using microtubule-associated protein 2 (MAP2) antibodies. Acta Neuropathol 97:13–21
12. Kusaka H, Matsumoto S, Imai T (1990) An adult-onset case of sporadic motor neuron disease with basophilic inclusions. Acta Neuropathol 80:660–665
13. Kusaka H, Matsumoto S, Imai T (1993) Adult-onset motor neu-ron disease with basophilic intraneuronal inclusion bodies. Clin Neuropathol 12:215–218
14. Kwiatkowski TJ Jr, Bosco DA, Leclerc AL et al (2009) Mutations in the FUS/TLS gene on chromosome 16 cause familial amyo-trophic lateral sclerosis. Science 323:1205–1208
15. Lagier-Tourenne C, Cleveland DW (2009) Rethinking ALS: the FUS about TDP-43. Cell 136:1001–1004
16. Matsumoto S, Kusaka H, Murakami N, Hashizume Y, Okazaki H, Hirano A (1992) Basophilic inclusions in sporadic juvenile amyotrophic lateral sclerosis: an immunocytochemical and ultrastructural study. Acta Neuropathol 83:579–583
17. Mizutani T, Sakamaki S, Tsuchiya N et al (1992) Amyotrophic lateral sclerosis with ophthalmoplegia and multisystem degener-ation in patients on long-term use of respirators. Acta Neuropathol 84:372–377
18. Munoz DG, Neumann M, Kusaka H et al (2009) FUS pathology in basophilic inclusion body disease. Acta Neuropathol 118:617–627
19. Munoz-Garcia D, Ludwin SK (1984) Classic and generalized variants of Pick's disease: a clinicopathological, ultrastructural, and immunocytochemical comparative study. Ann Neurol 16:467–480
20. Nelson JS, Prensky AL (1972) Sporadic juvenile amyotrophic lateral sclerosis. A clinicopathological study of a case with neu-ronal cytoplasmic inclusions containing RNA. Arch Neurol 27:300–306
21. Neumann M, Rademakers R, Roeber S, Baker M, Kretzschmar HA, Mackenzie IR (2009) Frontotemporal lobar degeneration with FUS pathology. Brain 132:2922–2931
22. Neumann M, Roeber S, Kretzschmar HA, Rademakers R, Baker M, Mackenzie IR (2009) Abundant FUS-immunoreactive pathology in neuronal intermediate filament inclusion disease. Acta Neuropathol 118:605–616
23. Nishihira Y, Tan CF, Hoshi Y et al (2009) Sporadic amyotrophic lateral sclerosis of long duration is associated with relatively mild TDP-43 pathology. Acta Neuropathol 117:45–53

24. Nishihira Y, Tan CF, Onodera O et al (2008) Sporadic amyotrophic lateral sclerosis: two pathological patterns shown by analysis of distribution of TDP-43-immunoreactive neuronal and glial cytoplasmic inclusions. Acta Neuropathol 116:169–182

25. Nonaka T, Kametani F, Arai T, Akiyama H, Hasegawa M (2009) Truncation and pathogenic mutations facilitate the formation of intracellular aggregates of TDP-43. Hum Mol Genet 18:3353–3364

26. Oda M, Akagawa N, Tabuchi Y, Tanabe H (1978) A sporadic juvenile case of the amyotrophic lateral sclerosis with neuronal intracytoplasmic inclusions. Acta Neuropathol 44:211–216

27. Piao YS, Wakabayashi K, Kakita A et al (2003) Neuropathology with clinical correlations of sporadic amyotrophic lateral sclerosis: 102 autopsy cases examined between 1962 and 2000. Brain Pathol 13:10–22

28. Rabbitts TH, Forster A, Larson R, Nathan P (1993) Fusion of the dominant negative transcription regulator CHOP with a novel gene FUS by translocation t(12;16) in malignant liposarcoma. Nat Genet 4:175–180

29. Rosen DR, Siddique T, Patterson D et al (1993) Mutations in Cu/Zn superoxide dismutase gene are associated with familial amyotrophic lateral sclerosis. Nature 362:59–62

30. Shaw CE, Enayat ZE, Powell JF et al (1997) Familial amyotrophic lateral sclerosis. Molecular pathology of a patient with a SOD1 mutation. Neurology 49:1612–1616

31. Sreedharan J, Blair IP, Tripathi VB et al (2008) TDP-43 mutations in familial and sporadic amyotrophic lateral sclerosis. Science 319:1668–1672

32. Tsuchiya K, Matsunaga T, Aoki M et al (2001) Familial amyotrophic lateral sclerosis with posterior column degeneration and basophilic inclusion bodies: a clinical, genetic and pathological study. Clin Neuropathol 20:53–59

33. Vance C, Rogelj B, Hortobagyi T et al (2009) Mutations in FUS, an RNA processing protein, cause familial amyotrophic lateral sclerosis type 6. Science 323:1208–1211

34. Wang X, Arai S, Song X et al (2008) Induced ncRNAs allosterically modify RNA-binding proteins in cis to inhibit transcription. Nature 454:126–130

35. Yang L, Embree LJ, Tsai S, Hickstein DD (1998) Oncoprotein TLS interacts with serine-arginine proteins involved in RNA splicing. J Biol Chem 273:27761–27764

36. Yoshida M, Murakami N, Hashizume Y, Itoh E, Takahashi A (1992) A clinicopathological study of two respirator-aided long-survival cases of amyotrophic lateral sclerosis. Rinsho Shinkeigaku 32:259–265